XL CILAMCE
IBERO-LATIN AMERICAN CONGRESS ON COMPUTATIONAL METHODS IN ENGINEERING
NOVEMBER 11-14, 2019
Praiamar Natal Hotel & Convention
Natal, RN-BRAZIL

NONLINEAR FINITE ELEMENT ANALYSIS OF UNBONDED PRESTRESSED CONCRETE BEAMS SUBJECTED TO SHORT-TERM LOADING

Juliana C. Alves
Evandro Parente Jr.
João Batista M. Sousa Jr.
julianacunhalves@gmail.com
evandro@ufc.br
joaobatistasousajr@hotmail.com
Laboratório de Mecânica Computacional e Visualização, Departamento de Engenharia Estrutural e Construcão Civil, Universidade Federal do Ceará, Campus do Pici, 60440-900, Fortaleza-CE, Brazil

Abstract. Prestressed concrete with unbonded tendons is an excellent structural solution for beams and slabs, allowing the design of slender elements with long spans. However, the consideration of the unbonded tendon in the structural analysis is complex, requiring the development and implementation of adequate methods. This work presents a finite element model formulation for material and geometric nonlinear analysis of unbonded prestressed beams. The Euler-Bernoulli nonlinear plane frame element formulation for large displacements and moderate rotations is used to model the reinforced concrete beam. The tendon is modeled as a single polygonal element with a variable number of straight segments. The tendon element allows the consideration of material and geometric nonlinearities. The formulation was successfully implemented and the obtained results were in good agreement with experimental data for beams with external and internal unbonded tendons. The presented formulation was applied to assess the influence of the geometric nonlinearity on the structural behavior of presstressed beams with unbonded tendons. The results showed that the geometric linear analysis overestimates the beam capacity.

Keywords: Prestressed concrete, Nonlinear analysis, Unbonded tendons

1 Introduction

Due to the low tensile resistance of concrete, crack formation is one of the main limiting factors in concrete element design. The presence of cracks in structures is responsible for exposing the reinforcement to corrosion compromising the durability and the element resistance. The use of prestressed tendons in concrete structures consists of an alternative to the use of traditional reinforced concrete since the stress applied tends to compress and bend before loading [1] preventing or limiting the crack formation under loading.

Several works were developed with the aim to simulate prestressed structures in its different systems. Among these approaches, there are studies with external prestressed concrete beams whose prestressing force is considered as an external loading [2–4] and as a resistance element[5–7].

Considering the cable as a resistance element allows adding the contribution of the tendon to the internal force vector and the stiffness matrix, as well as being a more realistic model, once the variation of tendon geometry throughout the analysis is also evaluated. Zona et al. [6] presented a study showing the effect of considering the geometric nonlinearity of the tendon. The incorporation of geometric nonlinearity in the model presented results closer to the experimental results. The disregard of these effects overestimates the strength of the structure. Also, Harajli et al. [4] presented a study where second-order effects are evaluated for externally prestressed concrete beams.

For beams with internal prestressing tendon, the prestressing may be bonded or unbonded. Unbonded prestressing concrete beams is the most used in the case of building structures, as it allows the use of slender elements, presenting simplicity and a higher rate of speed execution. Some works have been published to simulate this condition for short term loads [8]. While other studies considered, in addition to short-term loading, the behavior over time of unbonded prestressed concrete beams [9, 10].

In addition to computer simulations, some experimental tests were performed to study the behavior of partially prestressed beams [11]. Experimental studies have also been performed on beams for normal strength concrete and high strength concrete [12]. These studies are essential for the validation of models whose objective is to simulate prestressed concrete structures.

This work focus on exploring the model already presented by [8] for finite element analysis for material and geometric nonlinear analysis of prestressed concrete beams with unbonded internal tendons submitted to short-term loading. The reinforced concrete beam is modeled as a nonlinear Euler-Bernoulli frame element for large displacements and moderate rotations in a total Lagrangian approach. The tendon is modeled as a single polygonal element with a variable number of straight segments. In this work, the effect of the nonlinear strain-displacement relation is assessed as well as its effects on internal and external unbonded tendon prestressed concrete beams. Also, a physical interpretation of the tendon force over the frame element is presented.

The results presented a very good agreement with experimental data and shown that the nonlinear strain-displacements approach is significant of externally unbonded prestressed concrete elements since overestimates their capacities.

2 Frame element

For the reinforced concrete beam, the proposed model uses the Euler-Bernoulli frame element for large displacements and moderate rotations in a total Lagrangian approach. The hypothesis for Classical Beam Theory are adopted and displacements field is given by:

$$\begin{aligned} u(X,Y) &= u_0(X) - Y\, {v_0}' \\ v(X,Y) &= v_0(X) \end{aligned} \tag{1}$$

where u_0 e v_0 are the axial and transverse membrane displacements.

Considering moderate rotations, the strain field can be expressed in terms of its membrane strain ϵ_0 and curvature κ:

$$\epsilon = {u_0}' + \frac{1}{2}{v_0}'^2 - Y\, v'' = \epsilon_0 - Y\,\kappa \tag{2}$$

The membrane strain and the curvature are called generalized strains. In vector form:

$$\boldsymbol{\epsilon} = \begin{bmatrix} \epsilon_0 \\ \kappa \end{bmatrix} \tag{3}$$

The generalized strain vector presents a linear $\boldsymbol{\epsilon}_L$ and a geometric nonlinear $\boldsymbol{\epsilon}_{NL}$ portion:

$$\boldsymbol{\epsilon} = \boldsymbol{\epsilon}_L + \boldsymbol{\epsilon}_{NL} = \begin{bmatrix} {u_0}' \\ {v_0}'' \end{bmatrix} + \begin{bmatrix} \frac{1}{2}{v_0}'^2 \\ 0 \end{bmatrix} \tag{4}$$

The internal virtual work can be evaluated from strains and stresses in a volumetric body by the expression:

$$\delta U_e = \int_V \delta\boldsymbol{\epsilon}^T \boldsymbol{\sigma}\, \mathrm{d}V \tag{5}$$

where the strain increment can be written as:

$$\delta\epsilon = \delta\epsilon_0 - Y\,\delta\kappa \tag{6}$$

Then, since the plane frame element considers strains and stresses over the beam axis, the internal virtual work is given by:

$$\delta U_e = \int_V (\delta\epsilon_0 - Y\,\delta\kappa)\sigma_x\, \mathrm{d}V = \int_V \delta\boldsymbol{\epsilon}^T \boldsymbol{\sigma}\, \mathrm{d}X \tag{7}$$

Once the membrane and the curvature strain varies only over the segment length, it is possible to write the internal virtual work in function of the normal force N and bending moment M evaluated vy the integration of the stresses over the element cross-section:

$$\delta U_e = \int_L \big(\delta\epsilon_0\, N + \delta\kappa\, M\big)\mathrm{d}X \tag{8}$$

where

$$N = \int_A \sigma_x \mathrm{d}A \quad \text{and} \quad M \quad = -\int_A Y \sigma_x \mathrm{d}A \tag{9}$$

The generalized stresses can be written in vector form as:

$$\boldsymbol{\sigma} = \begin{bmatrix} N \\ M \end{bmatrix} \tag{10}$$

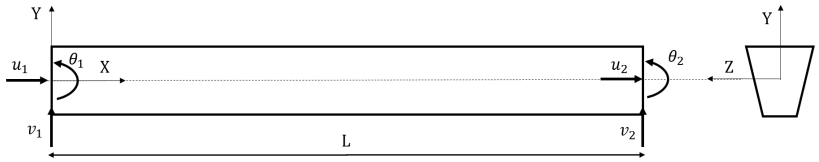

Figure 1. Frame element and degrees of freedom

For the interpolation of the axial and transverse displacements over the beam element, depicted in Figure 1, the minimum continuity required to be used is a C^0 linear and a C^1 cubic Hermitian interpolation functions, respectively. The introduction of the interpolation functions allows the representation of the strains over the element in terms of the displacements. The generalized strains can be written by using the strain-displacement matrices.

$$\epsilon = \mathbf{B}\mathbf{u}_e = \left(\mathbf{B}_L + \frac{1}{2}\mathbf{B}_{NL}\right)\mathbf{u}_e \tag{11}$$

where $\mathbf{B}_L$ and $\mathbf{B}_{NL}$ are the linear and nonlinear strain-displacement matrices, respectively, and $\mathbf{u}_e$ is the nodal element displacement vector. The term ${v_0}'$ can be written as:

$${v_0}' = \begin{bmatrix} 0 & {H_1}' & {H_2}' & 0 & {H_3}' & {H_4}' \end{bmatrix} \mathbf{u}_e = \mathbf{G}\mathbf{u}_e \tag{12}$$

Therefore, the nonlinear part of the membrane strain can be written as:

$$\epsilon_{NL} = \frac{1}{2}{v_0}' = \frac{1}{2}{\mathbf{u}_e}^T \mathbf{G}^T \mathbf{G}\mathbf{u}_e \tag{13}$$

Observe that this expression contains quartic terms since the linear portion of the strain is constant. There is an unbalance of the strain field, this can lead to membrane locking. In order to avoid the problem, Eq. (8) is substituted by the average nonlinear membrane strain [13]:

$$\epsilon_{NL} = \frac{1}{2}\frac{1}{L}\int_0^L {v_0}'^2 dX = \frac{1}{2}{\mathbf{u}_e}^T \mathbf{H}\mathbf{u}_e \tag{14}$$

where $\mathbf{H}$ is a symmetric constant matrix:

$$\mathbf{H} = \frac{1}{L}\int_0^L \mathbf{G}^T\mathbf{G}\,\mathrm{d}X \tag{15}$$

Thus, the nonlinear strain vector can be written:

$$\boldsymbol{\epsilon_{NL}} = \frac{1}{2}\begin{bmatrix} \mathbf{u}_e{}^T\mathbf{H}\mathbf{u}_e \\ 0 \end{bmatrix}\mathbf{u}_e = \mathbf{B}_{NL}\mathbf{u}_e \tag{16}$$

The strain increment $\delta\epsilon$ can be calculated as:

$$\delta\boldsymbol{\epsilon} = \Big(\mathbf{B}_L + \mathbf{B}_{NL}\Big)\delta\mathbf{u}_e = \bar{\mathbf{B}}\,\delta\mathbf{u}_e \tag{17}$$

where $\bar{\mathbf{B}}$ is the virtual strain-displacement matrix. Thus, it is possible to calculate the element internal force vector $\mathbf{g}_e$:

$$\delta U_e = \int_0^L \delta\boldsymbol{\epsilon}^T\boldsymbol{\sigma}\,\mathrm{d}X = \delta\mathbf{u}_e{}^T\int_0^L \bar{\mathbf{B}}^T\boldsymbol{\sigma}\,\mathrm{d}X = \delta\mathbf{u}_e{}^T\mathbf{g}_e \tag{18}$$

accordingly:

$$\mathbf{g}_e = \int_0^L \bar{\mathbf{B}}^T\boldsymbol{\sigma}\,\mathrm{d}X \tag{19}$$

The tangent stiffness matrix $\mathbf{K}_{Te}$ can be obtained by the differentiation of the internal force vector:

$$\mathbf{K}_{Te} = \frac{\partial\mathbf{g}_e}{\partial\mathbf{u}_e} = \mathbf{K}_{Ee} + \mathbf{K}_{Ge} \tag{20}$$

where $\mathbf{K}_{Ee}$ and $\mathbf{K}_{Ge}$ are the material stiffness matrix and the geometric stiffness matrix, respectively. The element material stiffness matrix is given by:

$$\mathbf{K}_{Ee} = \int_0^L \bar{\mathbf{B}}^T\mathbf{C}_T\bar{\mathbf{B}}\,\mathrm{d}X \tag{21}$$

where $\mathbf{C}_T$ corresponds to the tangent section constitutive matrix obtained from the generalized stresses vector:

$$\mathbf{C}_T = \frac{\partial\boldsymbol{\sigma}}{\partial\boldsymbol{\epsilon}} = \begin{bmatrix} \dfrac{\partial N}{\partial\epsilon_0} & \dfrac{\partial N}{\partial\kappa} \\ \dfrac{\partial M}{\partial\epsilon_0} & \dfrac{\partial M}{\partial\kappa} \end{bmatrix} \tag{22}$$

Finally, the element geometric stiffness matrix is given by:

$$\mathbf{K}_{Ge} = \int_0^L N\,\mathbf{H}\,\mathrm{d}X \tag{23}$$

Since the material of the concrete and reinforcement present nonlinear behavior, the cross-section stresses and their constitutive material matrix are evaluated using the fiber method. Also, for the integration over the element length, Gaussian quadrature with 2 points is performed.

2.1 Small displacements analysis

To evaluate the consideration of the geometric nonlinearity in the analysis of unbonded prestressed concrete beams, a small displacements formulation for the frame element is presented. This formulation adopts a linear strain-displacement relation and considers that the beam presents small displacements.

The displacements field is given by Eq. (1) and the linear strain field is given by:

$$\boldsymbol{\epsilon} = \boldsymbol{\epsilon}_L = \begin{bmatrix} {u_0}' \\ {v_0}'' \end{bmatrix} \tag{24}$$

The internal virtual work is given by the Eq.(**??**) where the internal forces are evaluated by the Eq. (9). Interpolation of the displacements field is carried out by the linear and hermitian interpolation functions for the axial (u) and vertical (v) displacements, respectively. Thus, the linear strain-displacement relation can be evaluated:

$$\boldsymbol{\epsilon}_L = \mathbf{B}\mathbf{u}_e \tag{25}$$

where $\mathbf{B} = \mathbf{B}_L$. Therefore, the strain increment can be written:

$$\delta\boldsymbol{\epsilon} = \mathbf{B}\,\delta\mathbf{u}_e \tag{26}$$

Thus, the element internal force vector $\mathbf{g}_e$ for the geometrically linear analysis:

$$\delta U_e = \int_0^L \delta\boldsymbol{\epsilon}^T\boldsymbol{\sigma}\,\mathrm{d}X = \delta\mathbf{u}_e{}^T\int_0^L \mathbf{B}^T\boldsymbol{\sigma}\,\mathrm{d}X \Rightarrow \mathbf{g}_e = \int_0^L \mathbf{B}^T\boldsymbol{\sigma}\,\mathrm{d}X \tag{27}$$

From the differentiation of the internal force vector in relation with the nodal displacements, it is possible to calculate the tangent stiffness matrix which corresponds to the material stiffness matrix:

$$\mathbf{K}_{Te} = \mathbf{K}_{Ee} = \int_0^L \mathbf{B}^T\mathbf{C}_T\mathbf{B}\,\mathrm{d}X \tag{28}$$

3 Unbonded tendon element

The prestressing tendon is modeled as a single polygonal element with a variable number of straight segments, as shown in Figure 2. It is important to note that unbonded tendons are coated in an anti-corrosion grease and protected by a plastic sheath. Due to the grease coating the friction between the cable and the sheathing can be neglected. Therefore, it is assumed that there is displacement compatibility between the sheating and the beam, but not between the cable and the sheating. This unbonded tendon element can be applied to the analysis of post-tensioned beams with internal (Figure 2a) and external tendons (Figure 2b).

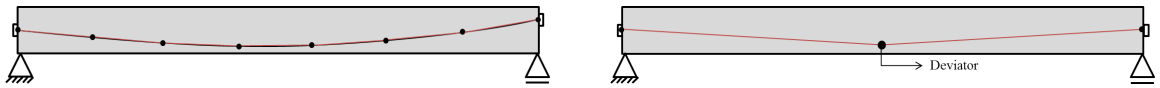

(a) Internal unbonded tendon (b) External unbonded tendon

Figure 2. Unbonded tendon element

Due to lack of strain compatibility, the tendon strain cannot be evaluated from beam cross-section displacements, but need to be evaluated considering the displacements of the whole cable. The cable displacements are evaluated from the displacements of the plastic sheathing, which is considered perfectly bonded to the concrete along the beam length for internal tendons and to the anchorage and deviator points for external tendons. Neglecting the friction between the plastic sheathing and the tendon, the strain along the tendon is uniform and, consequently, the tendon stress is constant.

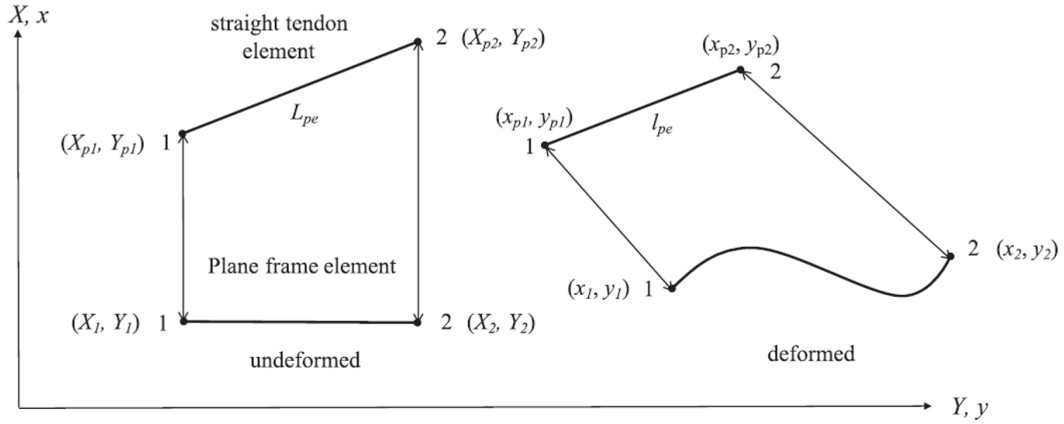

Figure 3. Frame element and unbonded tendon segment before and after the deformation

The displacement of the endpoints of each cable segment are related to the displacements of the corresponding beam nodes, as shown in Figure 3. Using Eq. (1), the displacement of these points can be written as

$$\begin{aligned} u_p(X_p, Y_p) &= u_0(X_p) - Y_p\,\theta(X_p) \\ v_p(X_p) &= v_0(X_p) \end{aligned} \tag{29}$$

where ($\theta = v_0'$) is the rotation of the beam element node and index p refers to the prestressing tendon. The current coordinates of the endpoints (x_p, y_p) can be evaluated adding these displacements to the initial coordinates (X_p, X_p).

The tendon segment displacements can be related to the frame element displacement as:

$$\begin{aligned} u_{p1} &= u_1 - Y_{p1}\,\theta_1 \\ v_{p1} &= v_1 \\ u_{p2} &= u_1 - Y_{p1}\,\theta_1 \\ v_{p2} &= v_2 \end{aligned} \tag{30}$$

In matrix form:

$$\begin{bmatrix} u_{p1} \\ v_{p1} \\ u_{p2} \\ v_{p2} \end{bmatrix} = \begin{bmatrix} 1 & 0 & -Y_1 & & & \\ 0 & 1 & 0 & & & \\ & & & 1 & 0 & -Y_2 \\ & & & 0 & 1 & 0 \end{bmatrix} \begin{bmatrix} u_1 \\ v_1 \\ \theta_1 \\ u_2 \\ v_2 \\ \theta_2 \end{bmatrix} \Rightarrow \mathbf{u}_{pe} = \mathbf{T}_e \mathbf{u}_e \tag{31}$$

where $\mathbf{u}_{pe}$ represents the nodal displacements vector of the tendon segment, $\mathbf{T}_e$ the transformation matrix, which depends on the ends coordinates of the undeformed segment, and $\mathbf{u}_e$ the nodal displacements vector of the frame element. Also, it is possible to relate the nodal displacements of the tendon segment to the global displacements vector of the frame element by applying the Boolean localization matrix $\mathbf{L}_e$ which relates the degrees of freedom of a tendon segment with the global degrees of freedom of the structure:

$$\mathbf{u}_e = \mathbf{L}_e \mathbf{u} \tag{32}$$

For a single tendon element whose initial length is L_p, and its deformed length is l_p, the element strain can be evaluated by using the engineering strain measure:

$$\epsilon_p = \frac{l_p - L_p}{L_p} \tag{33}$$

For a polygonal tendon composed by n straight segments:

$$L_p = \sum_{e=1}^{n_p} L_{pe} \quad \text{and} \quad l_p = \sum_{e=1}^{n_p} l_{pe} \tag{34}$$

The initial L_{pe} and final l_{pe} length of each tendon segment can be evaluated from the initial (undeformed) and current (deformed) coordinates of the segment endpoints:

$$L_{pe} = \sqrt{(X_{p2} - X_{p1})^2 + (Y_{p2} - Y_{p1})^2} \tag{35}$$

and

$$l_{pe} = \sqrt{(x_{p2} - x_{p1})^2 + (y_{p2} - y_{p1})^2} \tag{36}$$

The internal virtual work δU_p of the prestressing tendon element associated with its constant strain is given by:

$$\delta U_p = \int_0^{L_p} \int_0^{A_p} \delta\varepsilon_p \, \sigma_p \, \mathrm{d}A \, \mathrm{d}L = \delta\epsilon_p \, F_p \, L_p \tag{37}$$

where $\delta\epsilon_p$ is the tendon element virtual strain and F_p corresponds to the tendon force, given by:

$$F_p = \sigma_p \, A_p \tag{38}$$

The tendon strain is formed by the sum of the initial strain ϵ_0, which is constant, and the incremental displacement-dependent strain $\Delta\epsilon$:

$$\epsilon_p = \epsilon_{p0} + \Delta\epsilon_p \tag{39}$$

The incremental displacement-dependent strain is given by the sum of the individual strains of its n_p tendon segments. So, the Eq. (39) can be written as:

$$\epsilon_p = \epsilon_{p0} + \frac{\sum_{e=1}^{n_p} (l_{pe} - L_{pe})}{\sum_{e=1}^{n_p} L_{pe}} \tag{40}$$

To evaluate the virtual internal work, the strain variation $\delta\epsilon$ is determined from the Eq. (40):

$$\delta\epsilon_p = \frac{\delta l_p}{L_p} \tag{41}$$

Note that δl_p represents the variation of the deformed tendon element length formed by the sum of the deformed tendon segments length:

$$\delta l_p = \sum_{e=1}^{n_p} \delta l_{pe} \tag{42}$$

The variation of the final length of a tendon segment can be obtained from the expression of the final length of the tendon segment given by the Eq. (36):

$${l_{pe}}^2 = (x_{p2} - x_{p1})^2 + (y_{p2} - y_{p1})^2 \tag{43}$$

After some manipulation:

$$\delta l_{pe} = \cos\beta(\delta x_{p2} - \delta x_{p1}) + \sin\beta(\delta y_{p2} - \delta y_{p1}) \tag{44}$$

where β corresponds to the inclination angle with the horizontal axis of the deformed segment. The variation of a segment length also can be written in matrix form:

$$\delta l_{pe} = \begin{bmatrix} -\cos\beta & -\sin\beta & \cos\beta & \sin\beta \end{bmatrix} \begin{bmatrix} \delta u_{p1} \\ \delta v_{p1} \\ \delta u_{p2} \\ \delta v_{p2} \end{bmatrix} \Rightarrow \delta l_{pe} = \mathbf{r}_e^{\mathrm{T}} \delta \mathbf{u}_{pe} \tag{45}$$

where $\delta \mathbf{u}_{pe}$ corresponds to the virtual displacements of the tendon segment.

The variation of the element length δl_p corresponds to the sum of the segments length:

$$\delta l_p = \sum_{e=1}^{n_p} \delta l_{pe} = \sum_{e=1}^{n_p} {\mathbf{r}_e}^{\mathrm{T}} \mathbf{T}_e \delta \mathbf{u}_e \tag{46}$$

Finally, the internal virtual work of the unbonded tendon can be written:

$$\delta U_p = \delta \epsilon_p F_p L_p = \sum_{e=1}^{n_p} {\mathbf{r}_e}^{\mathrm{T}} \mathbf{T}_e \delta \mathbf{u}_e F_p \tag{47}$$

This expression can be written as:

$$\delta U_p = \sum_{e=1}^{n_p} {\mathbf{g}_{pe}}^{\mathrm{T}} \delta \mathbf{u_e} \tag{48}$$

where the internal force vector of each tendon segment can be calculated:

$$\mathbf{g}_{pe} = {\mathbf{T}_e}^{\mathrm{T}} \mathbf{r_e} F_p \Rightarrow \mathbf{g}_{pe} = \mathbf{w}_e F_p \tag{49}$$

Internal force vector can also be written as:

$$\mathbf{g}_{pe} = \begin{bmatrix} -\cos\beta \\ -\sin\beta \\ Y_{pi}\cos\beta \\ \cos\beta \\ \sin\beta \\ Y_{pj}\cos\beta \end{bmatrix} F_P \tag{50}$$

The tendon global internal force $\mathbf{g}_p$ can be evaluated as the sum of the contribution of its segments and from the Eq. (32):

$$\mathbf{g}_p = \sum_{e=1}^{n_p} {\mathbf{L}_e}^{\mathrm{T}} \mathbf{g}_{pe} \tag{51}$$

Figure 4a illustrates the representation of the decomposition of the tendon forces over the Cartesian axis, mathematically corresponding to $\mathbf{r}_e F_p$. In addition, Figure 4b represents the tendon forces over the beam element nodes, mathematically corresponding to $\mathbf{g}_{pe}$. These nodal forces includes a moment due to tendon eccentricity. Therefore, the internal force vector ($\mathbf{g}_{pe}$) consistently obtained by the virtual work approach can be interpreted as the effects of the tendon force F_p on the beam degrees of freedom.

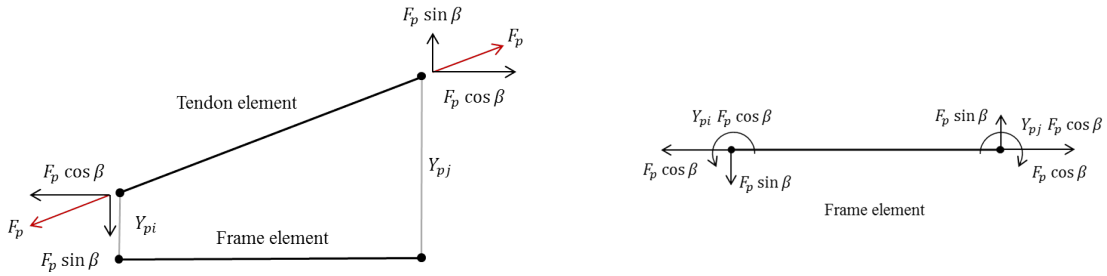

(a) Forces at segment ends ($\mathbf{r}_e F_p$)

(b) Equivalent tendon force ($\mathbf{w}_e F_p$)

Figure 4. Tendon equivalent forces over the frame element axis

From the differentiation of the global internal force vector with respect to the global nodal displacements, the tendon global tangent stiffness matrix $\mathbf{K}_{Tp}$ can be obtained:

$$\mathbf{K}_{Tp} = \frac{\partial \mathbf{g}_p}{\partial \mathbf{u}} = \sum_{e=1}^{n_p} {\mathbf{L}_e}^{\mathrm{T}} \frac{\partial \mathbf{g}_{pe}}{\partial \mathbf{u}} \tag{52}$$

The differentiation of the internal force vector of the segment is given by:

$$\frac{\partial \mathbf{g}_{pe}}{\partial \mathbf{u}} = \sum_{e=1}^{n_p} {\mathbf{L_e}}^{\mathrm{T}} \left({\mathbf{T}_e}^{\mathrm{T}} \frac{\partial \mathbf{r}_e}{\partial \mathbf{u}} F_p + {\mathbf{T}_e}^{\mathrm{T}} \mathbf{r}_e \frac{\partial F_p}{\partial \mathbf{u}} \right) \tag{53}$$

where the first term of the Eq. (53) corresponds to the geometric stiffness matrix and the second term corresponds to the material stiffness matrix.

The tendon force derivative is given by:

$$\frac{\partial F_p}{\partial \mathbf{u}} = A_p \frac{\partial \sigma_p}{\partial \epsilon_p} \frac{\partial \epsilon_p}{\partial \mathbf{u}} = \frac{A_p E_{pt}}{L_p} \sum_{a=1}^{n_p} {\mathbf{r}_a}^{\mathrm{T}} \mathbf{T}_a \mathbf{L}_a \tag{54}$$

where a indicates that the tendon force depends on the displacements of the whole prestressed tendon and E_{pt} is the tendon initial elastic modulus. Therefore, it is possible to evaluate the material stiffness matrix $\mathbf{K}_{E_p}$:

$$\mathbf{K}_{Ep} = \frac{A_p E_{pt}}{L_p} \mathbf{w}\mathbf{w}^{\mathrm{T}} \tag{55}$$

where:

$$\mathbf{w} = \sum_{e=1}^{n_p} {\mathbf{L}_e}^{\mathrm{T}} \mathbf{w}_e \tag{56}$$

From the Eq. (66), the derivative of its first term:

$$\frac{\partial \mathbf{r}_e}{\partial \mathbf{u}} = \frac{\partial \mathbf{r}_e}{\partial \mathbf{u}_e} \frac{\partial \mathbf{u}_e}{\partial \mathbf{u}} = \frac{\partial \mathbf{r}_e}{\partial \mathbf{u}_e} \mathbf{L}_e \tag{57}$$

with

$$\frac{\partial \mathbf{r}_e}{\partial \mathbf{u}_e} = \frac{\partial \mathbf{r}_e}{\partial \beta} \frac{\partial \beta}{\partial \mathbf{u}_{pe}} \frac{\partial \mathbf{u}_{pe}}{\partial \mathbf{u}_e} = \mathbf{z}_e \frac{\partial \beta}{\partial \mathbf{u}_{pe}} \mathbf{T}_e \tag{58}$$

where:

$${\mathbf{z}_\mathbf{e}}^T = \begin{bmatrix} \sin\beta & -\cos\beta & -\sin\beta & \cos\beta \end{bmatrix} \tag{59}$$

and

$$\frac{\partial \beta}{\partial \mathbf{u}_{pe}} = \frac{{\mathbf{z}_e}^{\mathrm{T}}}{l_{pe}} \tag{60}$$

Therefore, the geometric stiffness matrix of the tendon segment $\mathbf{K}_{Gpe}$ is calculated:

$$\mathbf{K}_{G_{pe}} = \frac{F_p}{l_{pe}} {\mathbf{T}_\mathbf{e}}^{\mathrm{T}} \mathbf{z}_e {\mathbf{z}_e}^{\mathrm{T}} \mathbf{T}_e \tag{61}$$

Finally, the global geometric stiffness matrix $\mathbf{K}_{G_p}$ is given by:

$$\mathbf{K}_{G_p} = \sum_{e=1}^{n_p} {\mathbf{L}_e}^{\mathrm{T}} \mathbf{K}_{G_{pe}} \mathbf{L}_e \tag{62}$$

The global tangent stiffness matrix of the tendon element can be expressed as the sum of the terms of the global material stiffness matrix given by Eq. (68) and for the global geometric stiffness matrix given by Eq. (62):

$$\mathbf{K}_{T_P} = \mathbf{K}_{E_p} + \mathbf{K}_{G_p} \tag{63}$$

3.1 Small displacements analysis

Assuming the hypothesis of small displacements, this section presents the formulation of a tendon element for linear geometric analysis. From the Eq. (45), it can be noticed that for a geometrically linear analysis, the tendon inclination angle β_0 is constant:

$$\delta l_{pe} = \mathbf{r}_{e0}^{\mathrm{T}} \delta \mathbf{u}_{pe} \tag{64}$$

where $\mathbf{r}_{e0}$ is the initial inclination tendon vector. Then, the internal force vector can be evaluated from the Eq. (47):

$$\delta U_p = \sum_{e=1}^{n_p} \mathbf{r}_{e0}{}^{\mathrm{T}} \mathbf{T}_e \delta \mathbf{u}_e F_p \quad \Rightarrow \quad \mathbf{g}_{pe} = \mathbf{T}_e{}^{\mathrm{T}} \mathbf{r}_{e0} F_p = \mathbf{w}_{e0} F_p \tag{65}$$

This expression shows that for geometrically linear analysis the tendon internal forces vary only due to the variation of the tendon force (F_p) since vector $\mathbf{w}_{e0}$ does not depend on the cable displacements.

From the expression of the internal force vector is possible to evaluate the tangent stiffness matrix for the geometrically linear tendon element:

$$\mathbf{K}_{T_P} = \frac{\partial \mathbf{g}_{pe}}{\partial \mathbf{u}} = \sum_{e=1}^{n_p} \mathbf{L_e}^{\mathrm{T}} \left(\mathbf{T}_e{}^{\mathrm{T}} \mathbf{r}_{e0} \frac{\partial F_p}{\partial \mathbf{u}} \right) \tag{66}$$

The differentiation of the tendon force with respect to the nodal displacements is given by:

$$\frac{\partial F_p}{\partial \mathbf{u}} = A_p \frac{\partial \sigma_p}{\partial \epsilon_p} \frac{\partial \epsilon_p}{\partial \mathbf{u}} = \frac{A_p E_{pt}}{L_p} \sum_{a=1}^{n_p} \mathbf{r}_{a0}{}^{\mathrm{T}} \mathbf{T}_a \mathbf{L}_a \tag{67}$$

Then, the tangent stiffness matrix, here equivalent to the material stiffness matrix, can be evaluated:

$$\mathbf{K}_{T_P} = \mathbf{K}_{Ep} = \frac{A_p E_{pt}}{L_p} \mathbf{w}_0 \mathbf{w}_0{}^{\mathrm{T}} \tag{68}$$

where:

$$\mathbf{w}_0 = \sum_{e=1}^{n_p} \mathbf{L}_e{}^{\mathrm{T}} \mathbf{w}_{e0} \tag{69}$$

Note that the subscribed 0 indicates that the inclination angle of the tendon segments are the undeformed inclinations angles ($\beta = \beta_0$). Its values are not actualized with the beam deformation, characterizing the linear geometric analysis.

4 Material Models

Several stress-strain relations have been proposed for simulating the nonlinear behavior of the steel and the concrete, although there is no agreement to which model performs the best fit to the experimental data available. The present work uses nonlinear uniaxial stress-strain relations for the concrete, the reinforcement steel, and the prestressing steel.

4.1 Concrete

Zupan and Saje [14] proposed a model for uniaxial relation for the concrete in compression and tension. The first range is from the ultimate compressive strain ϵ_{cu} to the strain corresponding to the tension resistance of the concrete ϵ_{ctr}. The second range corresponds to a straight line to the tensile resistance strain to the maximum tensile strain ϵ_{ctu}. The expression of the curve model is given by:

$$\sigma_c = \begin{cases} f_c \dfrac{2|\epsilon_{c0}|\epsilon_c}{{\epsilon_{c0}}^2 + {\epsilon_c}^2} & \epsilon_{cu} \leq \epsilon_c \leq \epsilon_{ctr} \\ \\ f_c \dfrac{\epsilon_c - \epsilon_{ctu}}{\epsilon_{ctr} - \epsilon_{ctu}} & \epsilon_{ctr} \leq \epsilon_c \leq \epsilon_{ctu} \end{cases} \tag{70}$$

Scott et al. [15] proposed curve for uniaxial relationship for the concrete was also considered. This model is formed of a parabolic ascending range and a linear descending range. The stress-strain relationship is given by:

$$\sigma_c = \begin{cases} f_c \left(\dfrac{2\epsilon_c}{0.002} - \left(\dfrac{\epsilon_c}{0.002} \right)^2 \right) & \epsilon_{cu} \leq 0.002 \\ \\ f_c \big(1 - Z(\epsilon_c - 0.002)\big) & \epsilon_c \geq 0.002 \end{cases} \tag{71}$$

where

$$Z = \frac{0.5}{\dfrac{3 + 0.29 f_c}{145 f_c} - 0.002} \tag{72}$$

4.2 Reinforcement and prestressing steel

For the reinforcement steel, a bilinear model is adopted for tension and compression, expressed by:

$$\sigma_s = \begin{cases} -f_y - E_{sh}(\epsilon_s + \epsilon_{sy}) & -\epsilon_{su} \leq \epsilon_s \leq -\epsilon_{sy} \\ E_s \epsilon_s & -\epsilon_{sy} \leq \epsilon_s \leq \epsilon_{sy} \\ -f_y - E_{sh}(\epsilon_s + \epsilon_{sy}) & \epsilon_{sy} \leq \epsilon_s \leq \epsilon_{su} \end{cases} \tag{73}$$

where E_{sh} is the steel hardening modulus, ϵ_{sy} is the yield strain, E_s the initial elastic modulus of the reinforcing steel.

For the prestressing steel, the constitutive relation proposed by Menegoto and Pinto [16] is adopted, where is valid only in tension, and given by:

$$\sigma_p = \epsilon_p E_p \left[Q + (1 - Q) \left(1 + \left(\frac{E_s \epsilon_p}{K \sigma_{py}} \right)^R \right)^{1/R} \right] \leq \sigma_{pu} \tag{74}$$

where E_p corresponds to the initial elastic modulus of the prestressing steel, Q, K and R corresponds to nondimentional coefficients that best fit to the material experimental data and σ_{py} is the prestressing steel yield stress.

5 Applications

This section presents the validation of the proposed formulation by comparison with available experimental results. Nonlinear analysis of three unbonded prestressed beams presenting different tendon profiles is performed. The results are evaluated in terms of the load-displacement curve obtained and the convergence of the Newton-Raphson iterations.

5.1 Unbonded prestressed beam with polygonal tendon profile

Hussien et al. [12] tested a set of unbonded prestressed beams. The beam named B7 is used to validate this model. B7 corresponds to a simply supported beam presenting a rectangular cross-section. The tendon profile, as shown in Figure 5, is anchored at the centroid of the ends cross-section and the lowest segment lies at 4.3 cm from the bottom of the beam. The tendon area is 0.99 cm^2 with a prestressing stress of 1000 MPa after the initial loses. The reinforcement steel is positioned at 4 cm from the top and bottom faces of the beam presenting 1.57 cm^2 each.

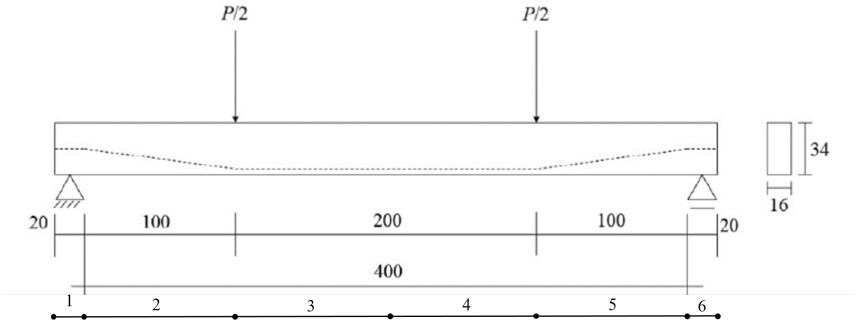

Figure 5. Unbonded prestressed beam tested by [12] (units in cm)

A set of parameters are presented in [12], namely: concrete compressive resistance 43 MPa, steel reinforcement yield 470 MPa, ultimate stress 610 MPa, yield stress for the prestressing tendon 1674 MPa and the ultimate prestressing stress 1860 MPa.

Figure 6. Load-displacement curve for beam B7

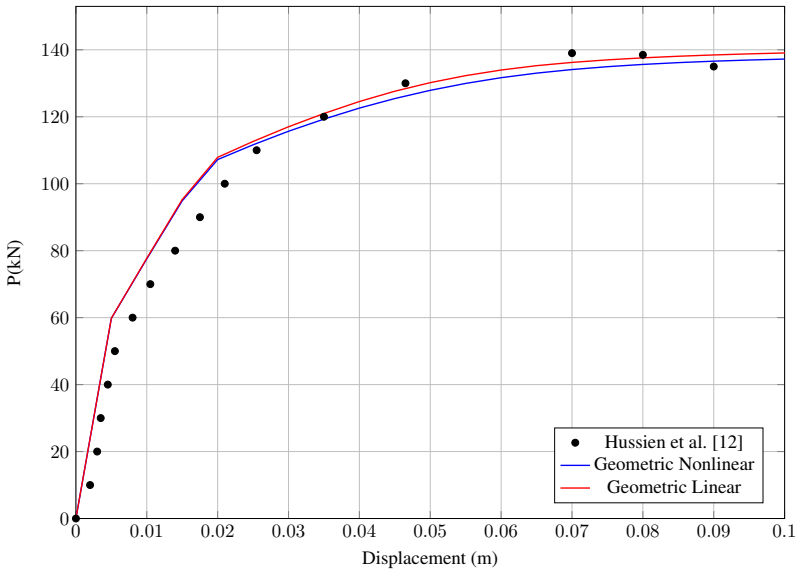

For the use of the nonlinear material models, a set of parameters are estimated. The peak compressive strain and the ultimate compressive strain was estimated, according to Eurocode guidelines, as

2.246×10^{-3} and 3.1×10^{-3}, respectively. For the use of the Zupan and Saje [14] uniaxial concrete model, the peak and ultimate tensile strains are estimated as 1×10^{-5} and 4×10^{-4}.

The reinforcement elastic modulus adopted is 210 GPa. The steel reinforcement ultimate strain estimated is 0.12 and hardening modulus 1.2GPa. The elastic modulus of the prestressing tendon adopted is 195GPa and the ultimate strain 0.06. The estimated parameters K, Q, and R for the prestressing steel model 1.04, 0.012 and 8.127, respectively.

The load-displacement curves are depicted in Figure 6. A 6 elements mesh was employed for the numerical analysis and the cross-section integration was performed using 50 layer. The displacement control method was used for nonlinear analysis, where the vertical displacement v of the central node of the beam was increased in 20 increments of 5 mm each. A tolerance for the Newton-Raphson iterations convergence of 10^{-5} was adopted.

The proposed formulation presented a very good agreement with the experimental results. Also, it is remarkable that the consideration of the nonlinear geometric behavior of prestressed concrete beams with unbonded internal tendon presents a small effect in the load-displacement curve. This behavior is already expected once the displacements of the tendon are linked with the concrete beam displacements, which presents small displacements.

Table 1 presents incremental results for the 20th step, corresponding to $v = 0.1$ mm. The results presented a fast convergence rate due to the correct implementation of the Newton-Raphson iterations for small and large displacements formulations, supporting the accuracy and consistency of the model. Also, it can be noticed that the small displacements formulation presents a higher force, overestimating the beam capacity in 1.5 %.

Table 1. Convergence 20th step for beam B7

	Nonlinear Geometric		Linear Geometric	
Iter	P (kN)	Error	P (kN)	Error
1	1.3726E+02	2.7275E+01	1.3904E+02	3.1722E-01
2	1.3722E+02	1.2051E-01	1.3906E+02	2.1106E-04
3	1.3722E+02	1.2622E-05	1.3906E+02	1.8895E-08
4	1.3722E+02	1.4773E-08	-	-

5.2 Unbonded prestressed beam with straight tendon profile

A set of prestressed beams with straight tendon profile was tested by Tao and Du [11]. The named A1 unbonded prestressed beam is simply supported with 4.20 spam and subjected to a four-point load as depicted in Figure 7. Cross-section rectangular with 16 cm wide and 28 cm deep. The concrete compression resistance is 30.6 MPa [11]. The peak compressive strain adopted is 2.021×10^{-3} and the ultimate compressive strain is 4.0×10^{-3}.

The lower reinforcement of 1.57 cm^2 is positioned at 25 cm from the superior face of the beam. The steel reinforcement parameters adopted for the yield stress is 267 MPa, the elastic modulus 210 MPa, the hardening modulus 1.2 GPa and the ultimate strain 0.16×10^{-4}.

The prestressing tendon of 0.588 cm^2 is positioned at 22 cm from the superior face of the beam. The prestressing parameters presented in [11] consists on the tendon stress of 960 MPa after initial loses, the elastic modulus 205 GPa, yield stress 1465 MPa, and ultimate stress 1790 MPa. The ultimate strain adopted for the prestressing steel is 0.06. The estimated coefficients K, Q and R for the tendon material model are 1.04, 0.02472, and 4.6019, respectively.

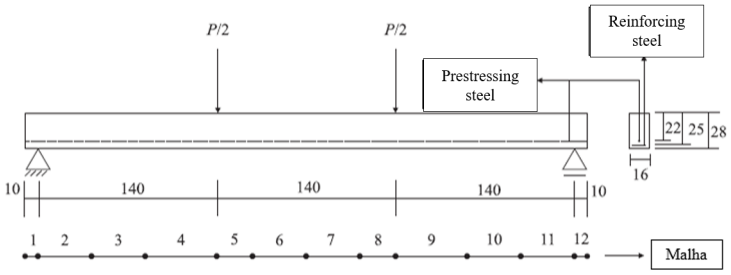

Figure 7. Unbonded prestressed beam tested by [11] (units in cm)

For the numerical analysis, the finite element mesh presents 12 frame elements and the transversal cross-section discretization presents 50 layers. The displacement method was applied for the central node whose displacement increment 1 mm for 20 increments was employed. The convergence tolerance adopted is 10^{-4}.

Figure 8. Load-displacement curve for the beam A1

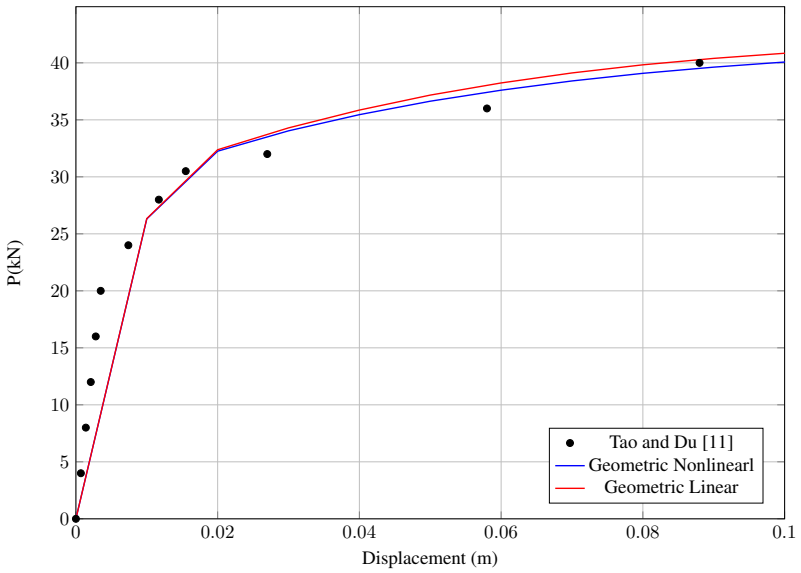

The Figure 8 shows the load-displacement curve at the mid-span obtained for the nonlinear and linear geometric analysis. It can be noted that the proposed formulation presents a very good agreement with the experimental results [11]. Over again, the geometric nonlinear behavior presents a small impact in the load-displacement curve.

Table 2. Convergence of 10th step for beam A1

	Nonlinear Geometric		Linear Geometric	
Iter	P (kN)	Error	P (kN)	Error
1	4.0118E+01	4.2478E+01	4.0777E+01	8.6423E-01
2	4.0072E+01	3.5758E+00	4.0842E+01	9.0076E-03
3	4.0072E+01	2.2147E-01	4.0842E+01	5.2828E-07
4	4.0072E+01	2.3680E-05	-	-

Table 2 presents the numerical results of the convergence of the 10th step ($v = 0.1$ m) for the dis-

placement control method. Again, the fast convergence of the Newton-Raphson iterations is observed for nonlinear and linear geometric analysis, showing the robustness of the proposed model. Also, the small displacements analysis overestimates the beam capacity in 2%. It can be noticed that for internal unbonded prestressed concrete beams, the small displacements analysis corresponds to a very good approximation, once the nonlinear geometric behavior presents a small effect in the beam capacity.

5.3 Externally prestressed concrete beam

Harajli et al. [4] performed an analytical nonlinear analysis for 12 externally prestressed concrete beams and presented a good agreement with the experimental results. The specimen named T1D is a simply supported T-beam with external prestressing tendon presenting one deviator at mid-span as depicted in Figure 9. The concrete strength is 40.8 MPa, and Scott et al. [15] stress-strain relation is used for simulating the concrete in compression.

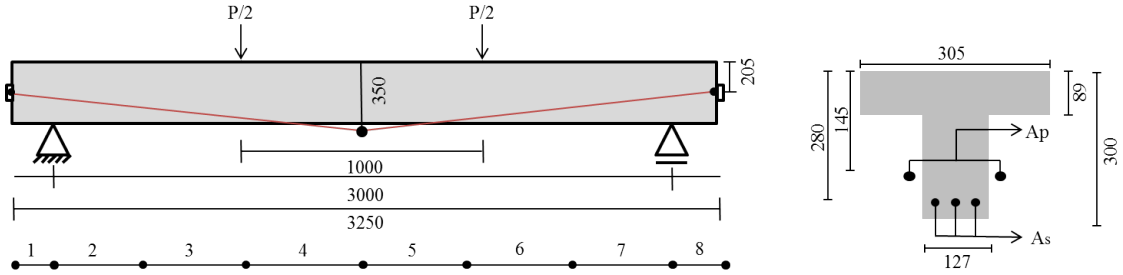

Figure 9. Externally prestressed concrete beam T1D studied by [4] (units in mm)

The reinforcement area corresponds to 2.26 cm^2 positioned at 205 mm from the top fiber. A bilinear stress-strain relation was used for modeling the compressive and tensile behavior of the reinforcing bars. The steel elastic modulus is 200 GPa and it was adopted a strain-hardening modulus equivalent a 1.5% of the elastic modulus [4]. The ultimate strain adopted is 0.15.

The prestressing steel is positioned at 280mm from the top fiber of the beam. The prestressing steel parameters presented in [4] consists on stress-strain model parameters for the curve proposed by Menegoto and Pinto [16], which the parameters K, Q, and R are 1.0618, 0.01174, and 7.344, respectively. Also, the prestressing steel yield stress 1.585 GPa, elastic modulus 193 GPa, and the ultimate stress 1427 MPa.

Figure 10. Load-displacement curve for beam T1D

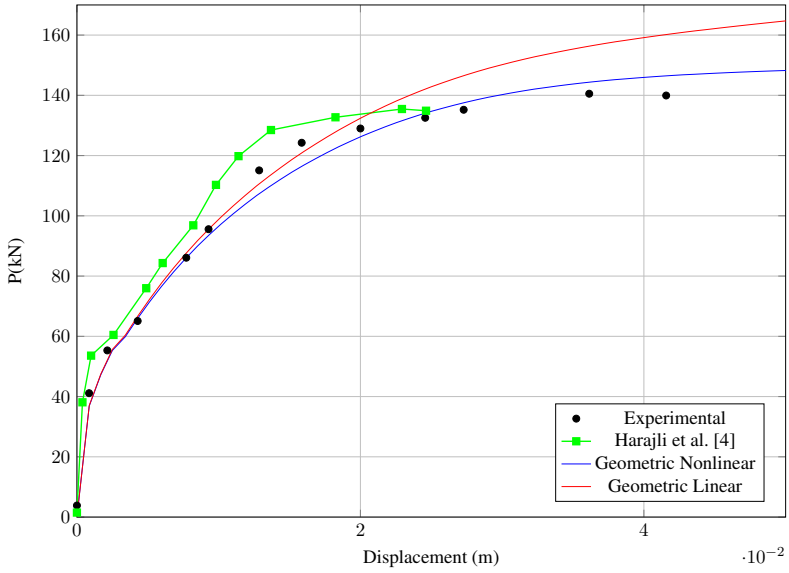

The finite element analysis was performed using 8 frame elements for the concrete beam and 1 tendon element with 2 segments to simulate the external prestressing. Section discretization consists of 25 layers. Displacement control method was applied using a displacement increment of 1mm for 40 increments. The convergence tolerance adopted was 10^{-4}.

Figure 10 depicts the load-displacement curve obtained for linear and nonlinear geometric numerical analysis. Note that the results obtained present a very good agreement with the experimental data. Also, perform a superior behavior compared to the analytical results evaluated by Harajil, capable of obtaining the complete load-displacement curve.

The load-displacement curves show that the nonlinear geometric behavior presented itself as a more expressive influence compared to the internal prestressed beams presented in the Section 5.2 and 5.3. This behavior is expected once the tendon lies externally from the beam and its is allowed to present a higher eccentricity, in contrast to the case of the internal tendon, where the plastic sheathing is considered perfectly bonded to the concrete.

The Table 3 presents the convergence of the 12th step for the displacement control method application. It can be noticed that for the externally prestressed concrete beam, the small displacements analysis leads to a significant increase of the beam capacity, around 12.3%.

Table 3. Convergence of the 12th step for the beam T1D

	Nonlinear Geometric		Linear Geometric	
Iter	P (kN)	Error	P (kN)	Error
1	1.4633E+02	1.2124E-04	1.6459E+02	1.2712E-03
2	1.4633E+02	1.8623E-06	1.6438E+02	2.9259E-04
3	-	-	1.6435E+02	6.6586E-06

6 Conclusions

A finite element model for geometric and material nonlinear analysis of unbonded prestressed concrete beams subjected to short term loading was presente. The reinforced concrete beam is simulated using nonlinear Euler-Bernoulli frame element for large displacements and moderate rotations. The prestressing tendon modeled as a single element composed of n_p segments. Material nonlinearity is also considered for concrete and steel by its stress-strain relations. Then, linear geometric analysis was performed by disregarded the nonlinear strain-displacement terms.

The global internal force vector and the tangent stiffness matrix are calculated in a consistent way. The proposed model was tested against experimental data presenting a very good agreement for the load-displacement curves obtained. In addition, the fast convergence of the Newton-Raphson iterations supports the reliability of the implementation.

The influence of the nonlinear geometric behavior of unbonded prestressed concrete beams was assessed for internall and external prestressed concrete elements presented in literature. The results presented excellent agreement with the experimental data. Also, the nonlinear geometric strain-displacements terms presented more effect on the beam capacity for externally prestressed members, overestimating their capacities.

Acknowledgements

This study was financed in part by the Coordenação de Aperfeiçoamento de Pessoal de Nível Superior - Brasil (CAPES) - Finance Code 001 and Conselho Nacional de Desenvolvimento Científico e Tecnológico (CNPq). This support is gratefully acknowledged.

References

[1] Aalami, B. O., 2014. *Post-Tensioned Buildings*. Cambridge University Press.

[2] Aalami, B. O., 1990. Load balancing. A comprehensive solution to post-tensioning. *ACI Structural Journal*, vol. 87, n. 6, pp. 662–670.

[3] jiong Lou, T. & qiang Xiang, Y., 2006. Finite element modeling of concrete beams prestressed with external tendons. *Engineering Structures*, vol. 28, n. 14, pp. 1919–1926.

[4] Harajli, M., Khairallah, N., & Nassif, H., 1999. Externally prestressed members evaluation of second-order effects. vol. 125, n. October, pp. 1151–1161.

[5] Aalami, B., 2000. Structural Modeling of Posttensioned Members. vol. 126, n. 2.

[6] Zona, A., Ragni, L., & Dall'Asta, A., 2008. Finite element formulation for geometric and material nonlinear analysis of beams prestressed with external slipping tendons. *Finite Elements in Analysis and Design*, vol. 44, n. 15, pp. 910–919.

[7] Lou, T., Lopes, S. M. R., & Lopes, A. V., 2013a. Flexural Response of Continuous Concrete Beams Prestressed with External Tendons. vol. 18, n. June, pp. 525–537.

[8] Moreira, L. S., Sousa, J. B. M., & Parente, E., 2018. Nonlinear finite element simulation of unbonded prestressed concrete beams. *Engineering Structures*, vol. 170, n. May, pp. 167–177.

[9] Lou, T., Lopes, S. M., & Lopes, A. V., 2013b. Nonlinear and time-dependent analysis of continuous unbonded prestressed concrete beams. *Computers and Structures*, vol. 119, pp. 166–176.

[10] Lou, T. & Karavasilis, T. L., 2018. Time-dependent assessment and deflection prediction of prestressed concrete beams with unbonded CFRP tendons. *Composite Structures*, vol. 194, n. March, pp. 365–376.

[11] Tao, X. & Du, G., 1985. Ultimate Stress of Unbonded Tendons in Partially Prestressed Concrete Beams. *PCI Journal*, vol. 30, n. 6, pp. 72–91.

[12] Hussien, O., Elafandy, T., Abdelrahman, A., Abdel Baky, S., & Nasr, E., 2012. Behavior of bonded and unbonded prestressed normal and high strength concrete beams. *HBRC Journal*, vol. 8, n. 3, pp. 239–251.

[13] Crisfield, M. A., 1991. *Non-linear finite element analysis of solids and structures*, volume 1. Wiley.

[14] Zupan, D. & Saje, M., 2005. Analytical integration of stress field and tangent material moduli over concrete cross-sections. *Computers and Structures*, vol. 83, n. 28-30 SPEC. ISS., pp. 2368–2380.

[15] Scott, B., Park, R., & Priestley, M., 1982. Stress-strain behaviour of concrete confined by overlapping hoops at low and high strain rates. *Journal of the American Concrete Institute*, vol. 79, pp. 13–27.

[16] Menegoto, M. & Pinto, P. E., 1973. Method of analysis for cyclically loaded R . C . plane frames including changes in geometry and non-elastic behaviour of elements under combined normal force and bending.